 doi:10.20944/preprints202105.0742.v1

Article

Thermal noise decoupling of micro-Newton thrust measured in a torsion balance

Lin-xiao Cong [1,2], Jian-chao Mu [1,2], Qian Liu [3], Hao Wang [2], Lin-lin Wang [3], Yong-gui Li [2] and Cong-feng Qiao [1,2*]

[1] School of Physical Sciences, the University of Chinese Academy of Sciences; clx@ucas.ac.cn;
[2] Key Laboratory of Vacuum Physics, the University of Chinese Academy of Sciences;
[3] National Space Science Center, the Chinese Academy of Sciences;
* Correspondence: qiaocf@ucas.ac.cn;

Abstract: The space gravitational wave detection and drag free control requires the micro-thruster to have very low thrust noise within 0.1mHz~100mHz, which poses a great challenge to the ground thrust test. The evaluation and decoupling of thermal noise are the difficulties in the application of torsion balance for most thrusters dissipate heat in the experiment. The research has adopted a calibration scheme of micro-Newton thrust torsion balance. On the basis of Lisa Pathfinder's former research and using ideas inspired from PID control and multi time scale (MTS) for reference, the paper proposes to expand the state space of temperature to be applied on thrust prediction based on fine tree regression (FTR), to subtract the thermal noise filtered by transfer function fitted with z-domain vector fitting (ZDVF). The results show that the thrust amplitude thrust density in diurnal temperature fluctuation is decoupled from 24μN/Hz$^{1/2}$ to 4.9μN/Hz$^{1/2}$ at 0.11mHz. And the 1μN square wave modulations of electrostatic fins (ESF) is extracted from the simultaneously ambiguous background of temperature for PTC's heating and cooling. The FTR method is well demonstrated in thermal noise decoupling and can guide the design of thermal control and be extended to other physical quantities for noise decoupling.

Keywords: thermal noise decoupling; micro-Newton thrust measurement; torsion balance; ZDVF; PID state extension; fine tree regression;

1. Introduction

The ultra-high precision requirements for micro-thrust performance in space-based gravitational wave detection [1,2], presents challenges to thrust measurement for thrusters of thrust-to-weight ratio (TWR) less than 10^{-9} [3,4]. In order to achieve a sub-micro-Newton level resolution, the calibrated thrust accuracy below 50μN should be better than 0.1μN on the ground. The instrument's thrust amplitude spectral density (ASD) should be less than 0.1μN/Hz$^{1/2}$ in the frequency band within 0.1mHz ~1Hz, and measurement background of thrust noise is strictly restricted for ultra-long period. Temperature variation leads to deformation of mechanical structure and output drift of electronic components, which are important factors affecting thrust accuracy and low frequency noise [5]. Due to the nonlinear response of hysteretic and asymmetric temperature variation [6] and its cross-coupling with multi-fields, the low-frequency thrust noise characteristics of torsion balance cannot be completely restored by fitting the transfer function and signal subtraction after filtering. Therefore, PID and MTS state expansion and tree regression model [7] are introduced to alleviate the thermal drift in torsion balance's thrust measurement, to subtract the displacement noise caused by temperature variation and to expand the deductible thermal impact bandwidth in the background noise.

 doi:10.20944/preprints202105.0742.v1

2. Setups and Methods

2.1. Thrust Balance Setup

Considering the TWR of the micro-thrust to be measured, the horizontal motion of the torsion balance can effectively isolate the impact of the thruster's gravitational weight on the measurement [8,9]. According to the objects of thrust balance, the balance can be divided into two modes: steady state measurement and dynamic measurement [10]. The former is to measure the displacement when the thrust is balanced with the deformation restoring force, and the latter is to calculate the closed-loop feedback force that nulls the torsion balance's deformation. In this paper, a torsion balance based on the deformation of the flexural pivot is discussed, which is more suitable for high-precision thrust calibration and low-frequency steady state measurement. The micro-deformation is observed by the capacitive displacement sensor, damped by eddy current from a copper plate and permanent magnet, and driven by the electrostatic force provided by the ESF [11,12]. As shown in Figure 1, the torsion balance is placed on an optical platform to isolate vibration, and sealed in a windshield to isolate turbulent air flow. PT1000 sensors of 0.01℃ resolution are equipped to study the thermal variation.

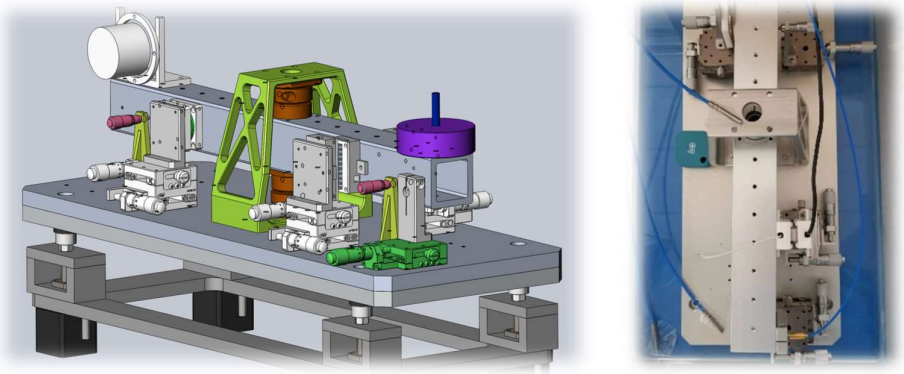

Figure 1 Overall structure design of torsion balance and its local view

2.2. Mathematical Model

The static measuring model of torsion balance is derived from the dynamic measuring model. As a response to thrust excitation, the position of torsional balance satisfies the second-order ordinary differential equation of deformation angle θ:

$$J\ddot{\theta} + c\dot{\theta} + K\theta = T \cdot L \tag{1}$$

where, J is the rotational inertia of torsional pendulum, c is the damping coefficient of the system, K is the torsional stiffness coefficient, T and L are the thrust to be measured and its acting moment arm length respectively. Take $s = j\omega$ as the differential operator, then the above can be resolved as:

$$\theta = \frac{T \cdot L}{Js^2 + cs + K} \tag{2}$$

When measuring the angular frequency $\omega = 2\pi f \to 0$, it can be obtained that the torsion balance satisfies the balance relation at rest:

$$\theta = \frac{T \cdot L}{K} = \frac{\Delta x}{r} \tag{3}$$

where, Δx is the displacement measured by torsion balance, r is the radius of arc angle corresponds to displacement, then the final thrust is:

Preprints (www.preprints.org) | NOT PEER-REVIEWED | Posted: 31 May 2021 doi:10.20944/preprints202105.0742.v1

$$T = \frac{K}{rL} \cdot \Delta x \tag{4}$$

The thrust can be then obtained by calibrating the coefficient K/rL of constant force. The thrust stiffness of torsional balance used in this study is estimated to be 7.56 μN/μm. However, the actual thrust response of torsion balance is not linear, such as the hysteresis of pivot torsion, the approximation of small angle, the non-parallel detection of capacitor, the coupling of ground vibration and noise, etc., which can cause the deviation of results. In particular, hot expansion and cold contraction of the structure caused by temperature variation will change the elastic coefficients of each component more or less, and the response curve calibrated by the electromagnetic sensor will drift, resulting in changes in the static balance position of the system as a result.

2.3. Decoupling Method

Whether signal and noise can be decoupled depends on the correlation between them and the understanding of the input and output of the system. Knowledge of the excitation changes or measurement of the response helps to control signal uncertainty. An intuitive way to evaluate the influence of unknown factors is to establish a function between independent and dependent variables based on the mechanism of action of physical factors. For example, by using ANSYS or COMSOL to study thermal influence on elastic elements with different properties, accurate and reliable mathematical models of temperature and physical characteristics of elastic elements are derived to provide theoretical guidance for compensating the thermal noise caused by temperature fluctuations. However, the above method relies on analytical calculation, which may be difficult to implement in reality due to the instability and non-linearity of some physical processes. Instead, it is universal to study the transfer function between excitation and response. Even when the numerical relationship is complex and it is difficult to establish a model, it can also analyze the data of the main interference factors and thrust in the environment, estimate the transfer function and deduct it quantitatively from the spectrum. A famous and widely used operation in LISA Pathfinder is to subtract the effect of temperature noise from laser interferometer signals. Specifically, the procedures are as followed [13]:

- transfer function
- Z-domain fit
- signal subtraction

For a discrete time system, the transfer function is defined by

$$H(z) = Y(z)X(z) \tag{5}$$

where X(z) and Y(z) are the z-transforms of the input x[n] and output y[n], respectively. The z-transform of a sequence x[n] is defined as

$$X(z) = \sum_{n=0}^{\infty} x[n]z^{-n} \tag{6}$$

where $z = e^{j\omega}$. For any pair of variables, their transfer function of time-series signals can be estimated by selecting region of interest (ROI) as analysis object. The concept of vector fitting (VF) and its algorithm was proposed to make rational approximation of frequency domain responses [14]. Z-domain vector-fitting (ZDVF) [15] is a formulation of vector-fitting method in the z domain, whose approximated output can be expanded in partial fractions:

$$F(z) = \sum_{n=1}^{N} \frac{r_n}{1 - p_n z^{-1}} \tag{7}$$

where r_n and p_n are residues and poles respectively. Each element of the partial fraction expansion can be seen as an IIR filter. This operation describes a recursive system that

 doi:10.20944/preprints202105.0742.v1

depends on current and past of the input x[n], but also on the output y[n]. The fitted filter is applied on the input to predict its output contribution, which will be subtracted from the original measured data.

However, complex heating process of the object and nonlinear temperature change reduce the degree of correlation with thrust, so it is necessary to first fit the dependent variable through regression learning in order to get better transfer characteristics. Thus, it is very important to find an optimal and reasonable regression algorithm in establishing the projection relationship between temperature and thrust.

2.4. Algorithm Optimization

The ZDVF can fit the equivalent filter of transfer function and reconstruct the thrust as response of the temperature excitation, then deduct the relevant thermal noise from the frequency domain. The hysteresis and nonlinearity of temperature can not be well treated by using temperature directly to estimate the thrust transfer function. By using regression learning to reduce the nonlinearity in latent space, better temperature to thrust correlation can be established numerically. For example, the least square regression method based on singular value decomposition (SVD) can modify the covariance, which has been proved to be valid in the data analysis of LISA Pathfinder's in-orbit experiments. Still, the model is limited by the uncertainty of physics boundary in the test process, including thermal response delay, temperature rebalance and hysteresis, so that the thrust's noise cannot be effectively deducted in a usual way. Multi-sensor fusion, variables' extension, MTS and FTR are introduced in the paper, and thermal noise is finally better fitted and subtracted. Specifically, modifications were made in the following aspects:

2.4.1. Extended state

The response of torsion balance to temperature is not real time output, and thermal modulation and response time change in different positions. In order to build an effective transfer function, the paper inherits the ideas of MTS and PID control, set different phase delays on the original temperature time series, combined with convolution, difference and other operations, so that temperature states on MTS (corresponding to frequency) can be extended. Then, based on multivariate statistical regression, the thrust fitted with PT1000 temperature was obtained, and the transfer function between the 'thrust' and the original thrust was built. So, thermal noise can be better evaluated and deducted in the thrust.

MTS [16] is short for multiple time scales, refer in particular to hierarchy of time steps corresponding to the hierarchy of frequencies in the system. The PT1000 time series are delay by full, half, 1/4 and 1/8 cycles of full time to cover different frequency variations. In addition, multi-sensor fusion which means a polynomial combination of temperature at different locations can improve the accuracy of transfer function. In theory, PT1000 can be distributed in all the locations that may be affected by the heat source. In consideration of the operation feasibility and the calculated quantity, 3 feature points near the torsion balance were selected during the experiment. Traditionally, PID control means feedback of proportional, integral and derivative of the process variable, which act on the deviation between set point and process variable. For the thermal effect on the system is cumulative and the displacement at present is correlated with the displacement at the previous time, integral can effectively eliminate static error. Here, we make the window function of four delay lengths, convolve the original data to carry out integration operation and calculate the difference between original data and delay data to extract trend variables. In this way, the PT1000 temperature data of the 3 points can be extended to proportional, integral and differential, and a richer data set with time and space universality can be constructed.

2.4.2. Regression learning

After the data preprocessing, the core work of regression learning is to develop and optimize the prediction model. Algorithms such as least square (LS), neural network (NN), principal component (PCA), support vector machine (SVM), decision tree, etc. can be used for regression learning. According to the prediction errors of different models for

 doi:10.20944/preprints202105.0742.v1

fitting thrust data, the effect of training can be evaluated. In this study, the difference between singular value decomposition-least square regression (SVD-LSR) algorithm and PID fine tree regression (PID-FTR) algorithm is compared. Specifically, we select the temperature extended time series in the training datasets, and PCA dimension reduction to overcome the collinear effect. Using thrust predicted by different models and the transfer function fit by ZDVF, thermal effect in the measured thrust output is estimated and decoupled by different filtering, and the expected thrust signal can be restored.

In detail, LSR is a global model based on a single predictive formula holding over the entire data-space. When the data has lots of features interacting in complicated, nonlinear ways, a single global model can be very difficult and confusing when you do succeed. An alternative way to nonlinear regression is to sub-divide, or partition, the space into smaller regions, where the interactions are more controlled. Tame chunks of the space can be fitted with simple models after recursive partitioning. The global model thus has two parts: the recursive partition and a simple model for each cell of the partition. FTR use the trees to represent the recursive partition. Each of the terminal nodes, or leaves, of the tree represents a cell of the partition, and has attached to it a simple model which applies in that cell only. A point x belongs to a leaf if x falls in the corresponding cell of the partition. The article will not expand FTR, but try to testify its use in thermal noise decoupling.

3. Results and Discussion

3.1. Diurnal Temperature Fluctuation

In order to provide a stable environment, the setup is placed on a passive vibration isolation optical platform and a windshield is used to prevent turbulence. The torsional stiffness coefficient of the flexural point is 0.245 Nm/rad, and the measuring moment arm was 0.18m, so as to record the displacement by a capacitive sensor with a resolution lower than 1nm at a sampling frequency of 5.21Hz. As shown in Figure 2, the temperature fluctuated between 24℃~28℃, and the thrust of the torsion balance fluctuated between 0 ~ 20μN after debias, showing a strong correlation with the diurnal alternation. As shown in Figure 3, the thrust noise amplitude spectral density is less than 1μN/Hz$^{1/2}$ at 1mHz, but up to 24μN/Hz at 0.12 mHz$^{1/2}$. The temperature change caused by thermal radiation of the sun amplifies the low frequency noise of the torsion balance below 1mHz.

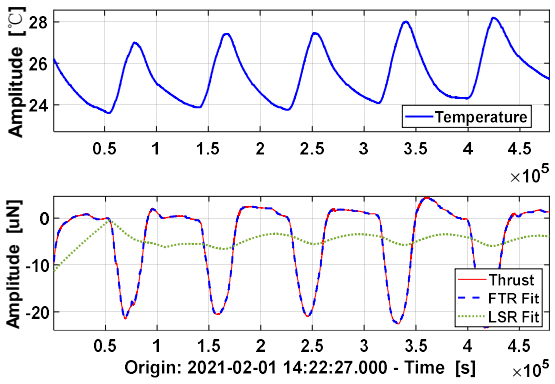

Figure 2 Synchronously collected temperature and displacement data

As the steps described earlier for thermal decoupling, displacement and temperature data are down-sampled to 0.1Hz before regression learning. As shown in Figure 2 below, the FTR fitted thrust (red dash line) is more accurate than that of LSR (green dot line), to predict the original the thrust and estimate transfer function. As shown in Figure 3, thrust ASD (T-ASD) decreased from 0.11mHz to 4.9μN/Hz$^{1/2}$ after temperature drift correction, reduced to 48μN/Hz$^{1/2}$ at 0.012mHz (24-hour), only 1/5th of the original. In addition, FTR

 doi:10.20944/preprints202105.0742.v1

has not only a larger amplitude decoupled than LSR does in fitting thermal thrust noise, but also a wider decoupled noise band of 1mHz larger than 0.1mHz of LSR. But for the limitation of the temperature sampling frequency and the modulation transfer amplitude of the position PT1000 located, the noise reduction effect in this experiment is not obvious above 1mHz, so shorter period temperature fluctuation is needed to testify.

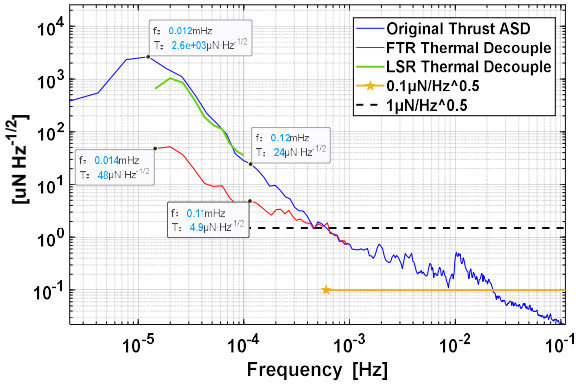

Figure 3 Spectral density of no-load thrust noise of torsion balance

3.2. Space-time Variation of Temperature

The thermal decoupling of thrust is to subtract thermal effect from the displacement, and the perturbation is propagated in oder of : heat source → PT1000 → torsion balance. The correlation between the PT1000 and the heat source is not the same as the that between the PT1000 and the torsion balance. Similarly, the correlation between the heat source and torsion balance is also not the same as between the PT1000 and torsion balance. As shown in Figure 4, the former is to build a model between the stability of the torsional balance's structure and the thermal deformation, i.e. which position is most likely to cause thrust thermal drift, paying attention to the structural sensitivity of torsional balance to PT1000 position. The latter is to bulid a heat conduction model from the heat source to PT1000, and pay attention to the thermal sensitivity of PT1000 position to the thermal source. Thus, an ideal temperature measuring point not only depends on the structure change of the torsion balance of PT1000 position, but also is closely related to the temperature changed by the heat source, for a good correlation with both sides is helpful to find the covariance and reduce thermal thrust noise.

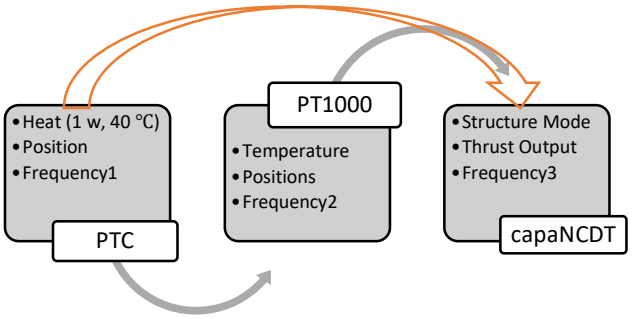

Figure 4 Transfer and measurement logic of thermal disturbance

The relationship between the heat source and the temperature of the PT1000 sensor is discussed first. In order to shorten the experiment time compared with diurnal exposure, a heating pad was laid on the bottom of the base of torsion balance, and the relay switch was triggered regularly. The temperature at the flexible pivot (T1), the base of the torsion balance (T2) and the glass plate of the torsion balance (T3) were recorded at the sampling

 doi:10.20944/preprints202105.0742.v1

frequency of 0.1Hz by heating for 2 minutes and turning off for 8 minutes. As shown in Figure 5, under the action of heat source, T3 is the first place to receive the heat and starts to rise periodically from 21℃ and gradually converges to around 25℃. The rise at T2 is delayed for the heat conduction is slower. But after heated up, the temperature converges to 26℃, which is higher than T3 and close to the heat source. T1 is furthest away from the heat source and has the smallest heat exchange area, thus the fluctuation during heating is the least. Because of the delay of heat, when one point is in a heating period, the other point may be in a cooling period. The heat dissipation rates at different locations of the system reflects the eigen frequency. Rising fast and falling slow, the temperature showed hysteresis characteristics when the structure is repeatedly heated, which also aggravates the deformation, stiffness degradation and energy consumption of the torsional balance structure in the process of thermodynamic equilibrium.

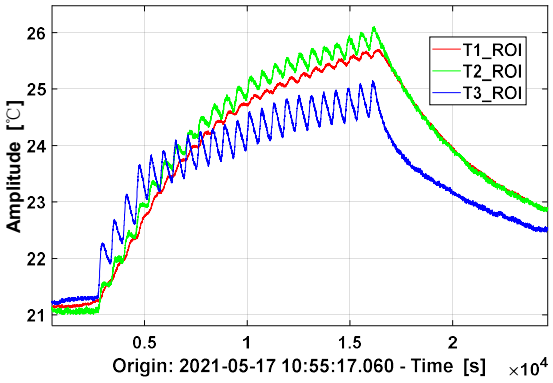

Figure 5 10-minute cycle heating data recorded by different temperature sensors

In the experiment above, a heating pad was used to heat the base of torsion balance, and the fluctuation of thrust balance was not obvious. In the next experiment, PTC heating was installed in the corner of the base below to lock the position that caused instability of the torsion balance. Regardless of the temperature of PT1000, to change the frequency of temperature fluctuations, PTC starts from turning on/off every 5 minutes at the beginning to turning on/off every 15 minutes and then to turning on/off every 30 minutes. The heat source square wave cycles range from 600 secs, 1800 secs and 3600 secs, corresponding to frequencies of 1.7mHz, 0.56mHz and 0.27mHz, respectively. As shown in Figure 6, the displacement data x_capaNCDT at 0.1mHz and 1mHz were subtracted to get a relative periodic result (red line): as the PTC work, the displacement modulation amplitude of the torsion balance increases gradually. There were two transient, high-frequency impulses during the experiment, one caused by passing people, the second by accidentally caught earthquake shock. In addition, it is found that the vibration mode of the optical platform switched in a period of 24 hours. During the rise from the evening to the next morning, the vibration of displacement at 0.02Hz is larger, which becomes weaker during the fall from the morning of the next day to the evening. The change is not related to PTC heating, but to the background noise of larger system and longer period.

In the frequency domain, the thrust ASD resolves peak signals at 0.26mHz, 0.52mHz and 1.7mHz, close to the PTC's modulated frequencies at 0.27mHz, 0.56mHz and 1.7mHz. The thermal noise at 0.26mHz is the largest, and noise at 1.7mHz is the smallest, and the frequency deviation of 0.52mHz is large due to the fewer sampling cycles. The modulation transfer function of temperature to displacement resembles a low-pass filter, and the ASD above 50mHz is less than 1μN/Hz$^{1/2}$, which provides a reference for the PT1000 sampling frequency. In addition, the heating position during the whole experiment is also a

 doi:10.20944/preprints202105.0742.v1

variable. The deformation of torsion balance is the direct cause of the fluctuation of thrust position, and the influence of the heat source is the indirect factor of thrust drift.

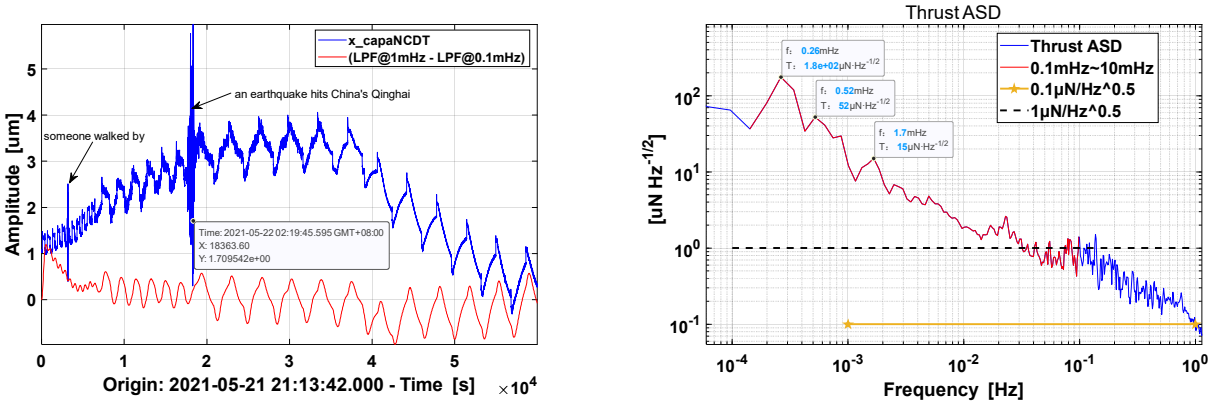

Figure 6 Displacement output of torsion balance at different heating frequencies of PTC

3.3. Square wave modulations of ESF and PTC

3.3.1. Temperature and displacement

The test of the micro thruster on the torsion balance is accompanied by the load heating, which makes the zero level of the force measured by the torsion balance drift as the time changes. In order to test this situation, the ESF (almost zero heat consumption) and PTC heating plate were used to synchronize the switch every half an hour to realize the temperature rise and fall, and thrust square wave with a period of one hour. At the same time, 3 sets of PT1000 were arranged to record temperature changes, and capacitive sensor was used to record the displacement of torsion balance.

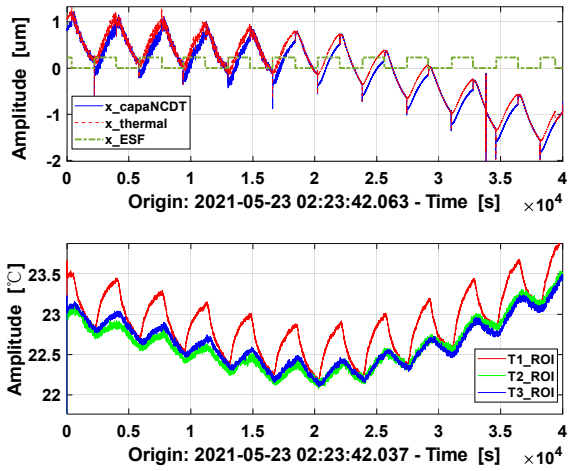

Figure 7 Displacement and temperature variation by square wave modulations of ESF and PTC

As shown in Figure 7, there seems a covariation between displacement (thrust) and temperature, but it is not a simple correlation. Before 3 x 10^4 s: Thrust and temperature move in accordance with each other in the modulated frequency, but also in the larger low-frequency trend; But after 3 x 10^4 s, although the temperature thrust is still correlated at the modulated frequency, the trend at lower frequencies is reversed. This is attributed to the fact that the heat balance of the system is determined not only by the modulated

Preprints (www.preprints.org) | NOT PEER-REVIEWED | Posted: 31 May 2021 doi:10.20944/preprints202105.0742.v1

frequency of PTC heating, but also by the larger system environment (including the platform) and the external temperature exchange. For example, PTC heating can cause the torsion balance to fluctuate briefly with the modulation period, but a longer-term trend is determined by the heating and deformation of basement platform. The height of the four corners of the base varies relative to each other because of thermal expansion and cold contraction. Usually, the gravitational weight of torsion pendulum will not produce a displacement, but when the platform tilts 1μrad, even a torsion bar of 0.1kg will produce 1μN as thrust increment, which needs to seek a new balance with flexible axis deformation. And 0.1μm difference between the ends of length 0.1m is enough to cause a horizontal change of 1μrad. The thermal deformation of the material is extremely difficult to control, and the problem is worse when the heat power of the thruster and other loads is added.

In addition, the square wave electrostatic thrust of ESF drift due to the temperature effect. According to the differential signal, the original displacement data (solid blue line in Figure 7 above) at the input square wave switch has a jump of about 0.23 μm, which corresponds to a thrust step of 1.7 μN. As the PT1000 at different locations are turned up or down due to the heat source, the temperature all rise or fall in varying ranges (below Figure 7). When the electrostatic thrust is constant, the displacement has a trend to change synchronously with the temperature. By completing the displacement data at the step, a relatively continuous thermal drift (red dashed line in Figure 7) can be approximated. To extract on the square wave signal in the huge background of thermal drift, assuming the electrostatic force be constant during the square wave, the temperature (T1_ROI, T2_ROI, T3_ROI) are first used to fit the displacement data x_thermal without electrostatic force. Then, based on the thrust predicted by regression learning, the transfer function from the fitted thrust to the thrust calculted by the displacement data x_capaNCDT is estimated via ZDVF, and the thermal drift in the electrostatic force measured by torsion balance is filtered out to restore the static force. The difference between the thermal thrust predicted by PID-FTR and SVD-LSR were compared. As shown in Figure 8, when fitting the thrust without ESF's electrostatic force, the PID-FTR algorithm learned the drift perfectly, while the SVD-LSR algorithm had high-frequency residuals and ultra-low frequency deviations. Compared to the thrust F_ROI calculated from the original displacement data, the fitted drift thrust based on FTR regression was clearly separated in time, while the thermal drift thrust based on LSR regression is now and then too close or too far.

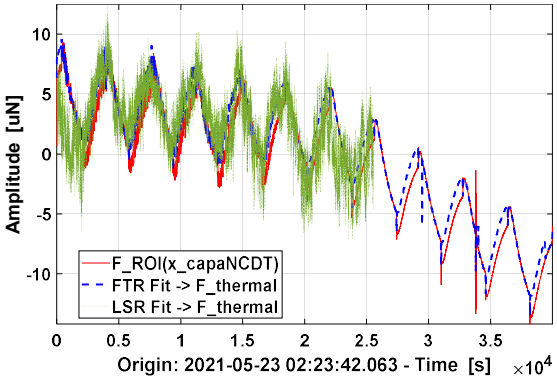

Figure 8 Comparison of fitting results between SVD-LSR and PID-FTR

3.3.2. Thermal noise decoupling

After fitting the thermal thrust caused by temperature, the following work returns to the normal procedure: transfer function, z-domain fit, and signal subtraction. It should be noted that meaningful frequencies should be selected when fitting the transfer function of

Preprints (www.preprints.org) | NOT PEER-REVIEWED | Posted: 31 May 2021 doi:10.20944/preprints202105.0742.v1

the system in z-domain. For the frequency of thermal thrust is low, the period interval of 20~ 2000 secs can be selected. As shown in Figure 9, the solid blue line (F_ROI) represents the original thrust ASD, and the solid red line (F_ROI - F_SQUARE) represents the ASD after the electrostatic force deducted. It can be seen that they are basically close to each other, but the difference lies in the square wave, where the potential signal is embedded in the area between the envelope of 1mHz ~ 10mHz. The blue and red dashed dotted line represent the thrust ASD results after FTR thermal thrust filtering, compared to the blue and red solid line respectively. When the electrostatic force is absent, the thrust ASD is decoupled and reduced below 1.5μN/Hz$^{1/2}$ in the full frequency band; even if the square wave is restored, it can be still locally reduced to 1.5μN/Hz$^{1/2}$ at 0.5mHz. What's different from the diurnal temperature variation, the thermal noise removal effect is more obvious near 10mHz except at the modulation frequency of 0.29mHz, while higher frequencies at 50mHz still have no thermal noise removed. It indicates that the temperature acquisition frequency about 0.1Hz is appropriate, and that the selection of temperature measurement points plays an important role in establishing the correlation between temperature and thrust drift of the torsion balance. Still, the results need to be verified by the restoration of electrostatic force in time domain again.

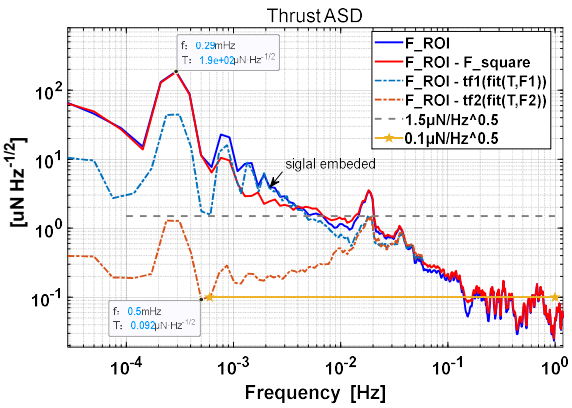

Figure 9 Thrust thermal noise decoupling with/without ESF

3.3.3. Restoration of electrostatic force

As mentioned above, PTC and ESF (10V voltage loaded) will be turned on and off at the same time every half an hour during the experiment. The ESF step output electrostatic force is 0.23μm×7.56μN/μm≈1.7μN. PTC heating makes the thrust characterized by the displacement of torsion balance drift gradually. As shown in Figure 10, after dealing with the PID-FTR and ZDVF series of algorithm, the thrust measurement result with thermal noise removed from the time domain can be seen clearly: ESF's real electrostatic force of 1.7μN square wave is extracted from the oscillations of 7μN affected by the temperature, along with the rising and falling template trigger position exactly. In addition to the electrostatic force, the recovered square wave retains vibrations other than thermal noise, such as the obvious 0.02 Hz vibration associated with the optical platform before 2×10^4 secs, which disappear again as expected after 2×10^4 secs. Therefore, the proposed process of thermal noise decoupling does not shave all the noise, but only removes the interference in the 0.5mHz ~ 50mHz related to temperature fluctuation, which is more real and more effective than the direct low-pass or band-pass filtering of displacement data.

It is a little confusing that in the electrostatic force restoration results after the removal of thermal noise, every step is accompanied by overshoot. To determine whether it is the residual error processed by the algorithm, the PTC was turned off in the contrast experiment, and the electrostatic square wave of 1μN turned on by the ESF alone, and the existence of "burr" can be observed. Through analysis, it is found that the signal of

Preprints (www.preprints.org) | NOT PEER-REVIEWED | Posted: 31 May 2021 doi:10.20944/preprints202105.0742.v1

capacitive displacement sensor is impacted by crosstalk in circuit switching when charging and discharging, and the thermal noise decoupling algorithm just retains this feature, which further demonstrates the effectiveness and pertinence of the algorithm.

In addition, both the time scale of FTR and the frequency range of ZDVF have the risk of underfitting or overfitting. As for the tuning of relevant parameters, on the one hand, the range of frequency coverage should be taken into account, and the adjustment should be made according to mean square error to obtain better fitting results. On the other hand, the spectral response of the actual physical quantity should also be used to iterate according to the thermal noise subtraction effect, and cross validated through a priori template (such as square wave). In general, datasets of different variation modes can be added to train the temperature's prediction ability of the FTR model. The noise decoupling precision of ZDVF can be refined and enhanced by using different frequency modulation of temperature and different location acquisition temperature.

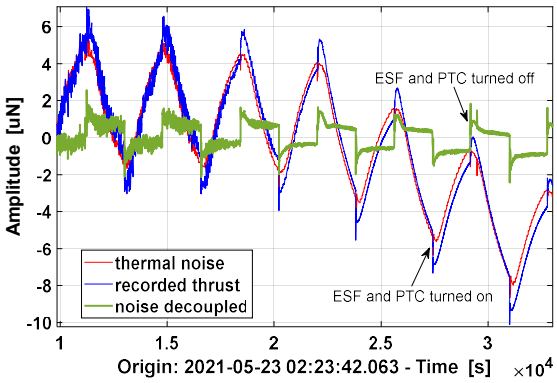

Figure 10 Thermal noise decoupled to find square wave signal

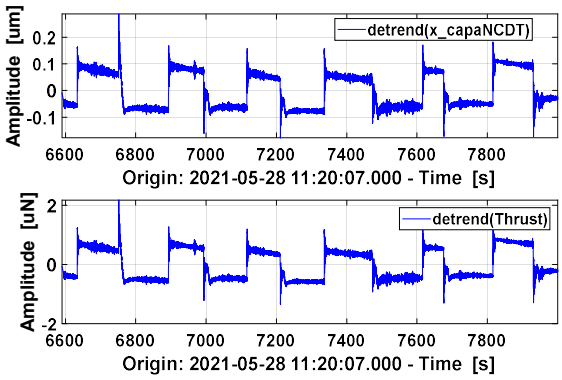

Figure 11 Open the ESF separately to output 1μN square wave of electrostatic force

4. Conclusions

The thermal noise removal of torsion balance is a tricky problem in micro-Newton-level thrust measurement, for the nonlinearity and hysteresis of temperature in the thrust output is hard to cope with. In addition to the analytical method to explore the mechanism of temperature action, it is easier to understand the thermal noise in terms of data stream of the system, such as ZDVF used to fit the thrust transfer function and filter the thermal noise in the original results. To enhance the correlation between thrust and temperature, a new fitting method based PID states extension and fine tree regression was proposed in

the paper. The new algorithm showed a great potential in thermal noise decoupling, such as decreasing the peak thrust ASD of temperature variation, or extracting the ESF's 1.7μN square wave from a thermal drift up to 7μN. In essence, the projection to latent structure help find the linear thrust response of the temperature, and PID-FTR regression learning contributed to that. In the future, the focus of thermal noise decoupling is to enrich the diversity of training datasets, to enhance the transportability and computation efficiency of prediction models, and to guide the thermal control design based on low noise modes. The final goal is to keep the measurement thrust ASD lower than $0.1\mu N/Hz^{1/2}$ at 0.1mHz, which will be possible with the help of other thermal control methods.

Acknowledgements: This work was supported in part by the Strategic Priority Research Program of Chinese Academy of Sciences (CAS) under Contracts Nos. XDA1502070504, and the Major Scientific Instrument and Equipment Development Project of CAS under the Grants E0EK0201.

Conflicts of Interest: The authors declare no conflict of interest.

References

1 McNamara, Paul W. (2012). The LISA pathfinder mission. International Journal of Modern Physics D, 22(01), 1341001-.

2 Hu W.R. , &Wu Y.L. (2017).The Taiji Program in Space for gravitational wave physics and the nature of gravity. National science review,4(5),685-686.

3 Luo, Z. , Wang, Y. , Wu, Y. , Hu, W. , & Jin, G. . (2020). The Taiji program: a concise overview. Progress of Theoretical and Experimental Physics.

4 Xu, S. Y. , Xu, L. X. , Cong, L. X. , Li, Y. G. , Qiao, C. F. & On behalf of The Taiji Scientific Collaboration. (2021). First result of orbit verification of taiji-1 hall micro thruster. International Journal of Modern Physics A.

5 Lee C. , Kim G. , Yi C., B L Musicó, & Liaw P. K. (2020). Temperature dependence of elastic and plastic deformation behavior of a refractory high-entropy alloy. Science Advances, 6(37).

6 Vavra, & Marian. (2013). Testing for non-linearity and asymmetry in time series. Birkbeck.

7 Huang, M. L. , & Lin, Y. J. . (2020). Regression tree model for predicting game scores for the golden state warriors in the national basketball association. Symmetry, 12(5), 835.

8 Kolbeck, J. , Porter, E. , & Keidar, M. . (2017). High Precision Thrust Balance Development at The George Washington. International Electric Propulsion Conference 2017.

9 Little, B. , & Jugroot, M. . (2019). Development of a microthrust balance and ion beam measurement system: characterizing a dual-mode thruster for spacecraft. Vacuum.

10 Yang, C. , He, J. W. , Duan, L. , Kang, Q. , & On behalf of The Taiji Scientific Collaboration. (2021). A torsional thrust stand for measuring the thrust response time of micro-newton thrusters. International Journal of Modern Physics A.

11 Johnson, W. A. , & Warne, L. K. . (1995). Electrophysics of micromechanical comb actuators. Journal of Microelectromechanical Systems, 4(1), 49-59.

12 Yan, A. , Appel, B. , & Gedrimas, J. . (2006). MilliNewton Thrust Stand Calibration Using Electrostatic Fins. Aiaa Aerospace Sciences Meeting Including the New Horizons Forum & Aerospace Exposition.

13 IFO/Temperature Example - signal subtraction (LTPDA Toolbox) (lisamission.org)

14 B. Gustavsen and A. Semlyen, "Rational approximation of frequency domain responses by Vector Fitting", IEEE Trans. Power Delivery vol. 14, no. 3, pp. 1052-1061, July 1999.

15 Y. S. Mekonnen and J. E. Schutt-Aine, "Fast broadband macromodeling technique of sampled time/frequency data using z-domain vector-fitting method", Electronic Components and Technology Conference, 2008. ECTC 2008. 58th 27-30 May 2008 pp. 1231 - 1235.

16 Iacobelli S, Carstensen B. Multiple time scales in multi-state models. Stat Med. 2013 Dec 30;32(30):5315-27. doi: 10.1002/sim.5976. Epub 2013 Sep 12. PMID: 24027131.